

# Non-thermal radiation from a runaway massive star

Gustavo E. Romero<sup>1,2</sup>, Paula Benaglia<sup>1,2</sup>, Cintia S. Peri<sup>1,2</sup>,  
Josep Martí<sup>3</sup>, Anabella T. Araudo<sup>1,2</sup>

<sup>1</sup> Instituto Argentino de Radioastronomía, CCT-La Plata, CONICET,  
C.C.5, (1894) Villa Elisa, Buenos Aires, Argentina

<sup>2</sup> Facultad de Ciencias Astronómicas y Geofísicas UNLP,  
Paseo del Bosque S/N, B1900FWA La Plata, Argentina

<sup>3</sup> Departamento de Física (EPS), Universidad de Jaén, Campus Las Lagunillas s/n, 23071 Jaén, Spain

**Abstract:** We present a study of the radio emission from a massive runaway star. The star forms a bow shock that is clearly observed in the infrared. We have performed VLA observations under the assumption that the reverse shock in the stellar wind might accelerate charged particles up to relativistic energies. Non-thermal radio emission of synchrotron origin has been detected, confirming the hypothesis. We have then modeled the system and we predict a spectral energy distribution that extends up to  $\gamma$ -rays. Under some simplifying assumptions, we find that the intensity at high energies is too low to be detected by current instruments, but the future Cherenkov Telescope Array might detect the source.

## 1 Introduction

Runaway OB stars (Gies and Bolton 1986) can produce so-called stellar bow shocks on the surrounding interstellar medium. Bow shocks develop as arc-shaped structures, with bows pointing in the same direction of the stellar velocity, while the star moves supersonically through the interstellar medium (ISM). The stellar and shock-excited radiation heat the dust and gas swept by the bow shock. The dust, in turn, re-radiates the energy as mid to far IR flux.

Van Buren & McCray (1988) looked for bow-shaped features near high-velocity O stars and found an IR candidate close to the O supergiant BD+43°3654 ( $\alpha, \delta$ [J2000] =  $20^{\text{h}}33^{\text{m}}36.077^{\text{s}}, +43^{\circ}59'07.40''$ ;  $l, b = 82.41^{\circ}, +2.33^{\circ}$ ). Comerón & Pasquali (2007) related the star BD+43°3654 to a bow shock detected with the Midcourse Space eXperiment (MSX) at D and E bands. Also, data from the NRAO-VLA<sup>1</sup> NVSS Survey (Condon et al. 1998) revealed a coma-shaped source of  $\sim 7$  arcmin spatially coincident with the MSX feature (Figure 1).

A radio study of the bow shock can shed light on the physical processes that give rise to high-energy emission from a stellar source, regardless of the history of the runaway star. The shock can accelerate particles up to relativistic energies by Fermi mechanism. Energetic electrons will cool through synchrotron radiation, producing a non-thermal radio source. We carried out radio observations at two frequencies to study the nature of the emission from the bow shock of BD+43°3654.

<sup>1</sup>National Radio Astronomy Observatory - Very Large Array (<http://www.vla.nrao.edu/>).

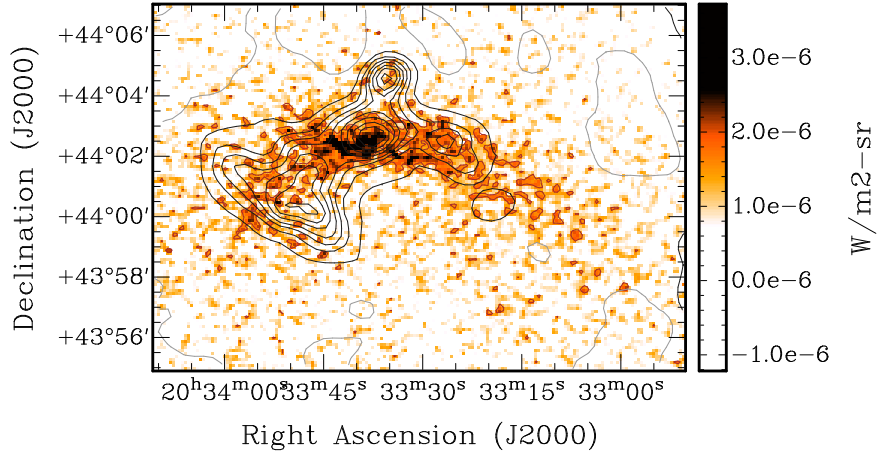


Figure 1: MSX-D band image (color scale) superposed to 1.4 GHz-NVSS contours. Levels are:  $-2$ ,  $2$  ( $2\sigma$ ),  $5$ ,  $8$ ,  $11$ ,  $15$ ,  $19$ ,  $24$ ,  $29$ ,  $50$ ,  $70$ , and  $90$   $\text{mJy beam}^{-1}$ .

## 2 Observations and results

Our continuum observations were carried out with the Very Large Array (VLA) at 1.42 GHz (C config.) and at 4.86 GHz (D config.). Figure 2 presents the resulting images after primary beam correction, re-gridded with the same synthesized beam of  $12''$ . There is emission at both frequencies along the extension of the MSX source. The hypothesis of a physical association between the star and the radio/IR features is supported by the very good agreement of the residual proper motion of the star and the direction from the star to the apsis of the bow shock (Fig. 2). We used the continuum images

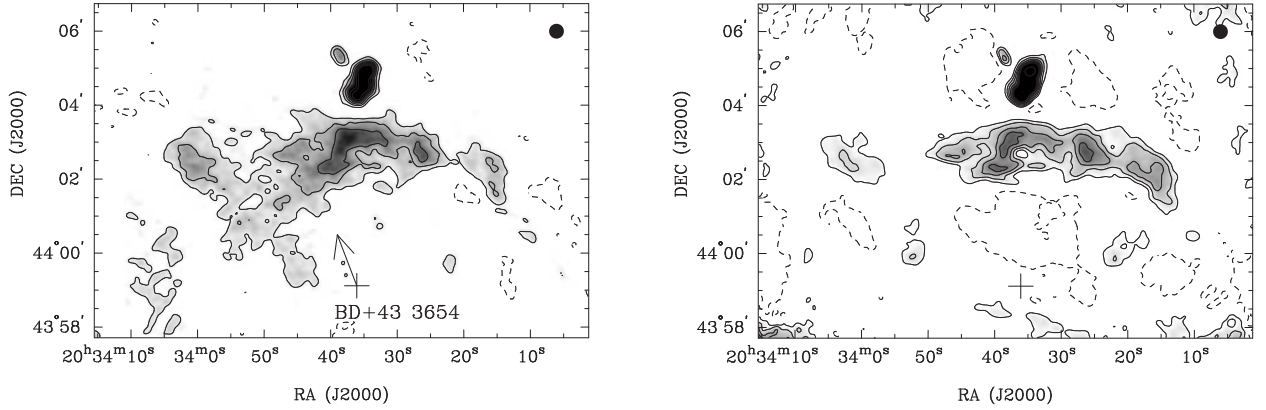


Figure 2: Continuum emission at 1.42 GHz (left), and at 4.86 GHz (right). Contour levels are  $-3$ ,  $3$ ,  $6$ ,  $10$ ,  $15$ ,  $20$ ,  $25$ , and  $60$  times the rms of  $0.3$  and  $0.2$   $\text{mJy beam}^{-1}$ . BD+43° 3654 is marked with a cross. The arrow represents the velocity vector of the star, derived from proper motions corrected for local motion of the surrounding ISM (see text). Synthesized beams of  $12'' \times 12''$  are shown in the top right corners.

at 1.42 and 4.86 GHz to build a spectral index distribution map. We only considered input pixels with a signal-to-noise ratio  $\geq 4$ . Besides, the spectral index map was masked for a signal-to-noise ratio  $\geq 10$ . Figures 3 and 4 show the spectral index distribution and corresponding noise maps.

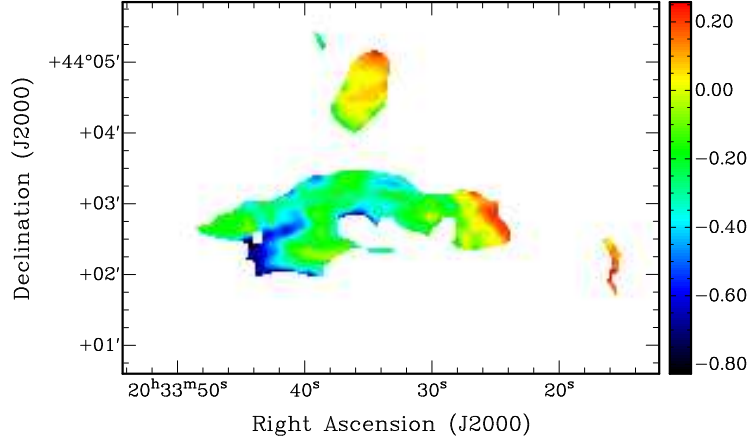


Figure 3: Spectral index distribution.

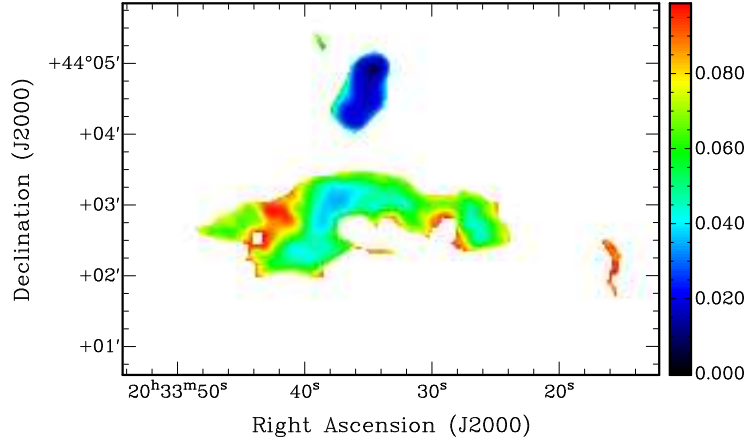


Figure 4: Spectral index error distribution.

### 3 Bow-shock emission

Most of the area shows a source of non-thermal radiation with index  $\langle \alpha \rangle = -0.5$  ( $S_\nu \propto \nu^\alpha$ ), as obtained from the VLA data. We adopted a distance to the bow-shock of 1.4 kpc (Hanson 2003). The distance from the star to the bow-shock is  $R = 5'$ , or 2 pc. The volume occupied by the bow-shock is  $\sim 4.6 \text{ pc}^3$ . We took a particle density of the ISM in the bow shock region of  $100 \text{ cm}^{-3}$  (see Kobulnicky et al. 2010).

The non-thermal radiation is expected from synchrotron emission generated by relativistic electrons accelerated either at the forward shock in the ISM or in the reverse shock in the stellar wind. We estimated the particle energy distribution ( $n$ ) using the observed flux density and spectral slope, and assumed equipartition between magnetic and relativistic particles energy density.

We considered that the energy density of relativistic particles has three contributions:

$$u = u_{e_1} + u_p + u_{e_2} = \int E_{e_1} n_{e_1}(E_{e_1}) dE_{e_1} + \int E_p n_p(E_p) dE_p + \int E_{e_2} n_{e_2}(E_{e_2}) dE_{e_2}, \quad (1)$$

where  $e_1$ ,  $p$ , and  $e_2$  stand for relativistic primary electrons, protons, and secondary electron-positron pairs (i.e. pairs coming from charged pion decays), respectively. The relation between primary electrons and protons energy density is  $u_p = a u_{e_1}$ , with  $a \geq 0$ . Three cases were considered:  $a = 0$  (just electrons),  $a = 1$  (equal energy density in both species), and  $a = 100$  (proton-dominated case, as observed in the galactic cosmic rays). The magnetic field resulted  $B \sim 5 \times 10^{-5} \text{ G}$ .

The maximum energy of the particles was determined by balancing energy gains and losses. The loss mechanisms considered were (i) synchrotron radiation, (ii) relativistic Bremsstrahlung, (iii) particle escape from the radiation region due to convection by the stellar wind, and (iv) inverse Compton (IC) scattering of IR, stellar and cosmic microwave background photons. In the case of protons, the only relevant losses are proton-proton ( $pp$ ) inelastic collisions and convective escape. Diffusion is negligible in comparison to convection in this situation (the respective timescales are  $t_{\text{conv}} \sim 6 \times 10^6$  s and  $t_{\text{diff}} \sim 10^{13}/(E/\text{erg})$  s). Both primary electrons and protons reach energies up to  $\sim 10^{13}$  eV, which is imposed by non-radiative losses, except for  $a = 100$ , where synchrotron losses dominate for electrons. Figure 5 shows the losses for electrons and protons in the case  $a = 1$ .

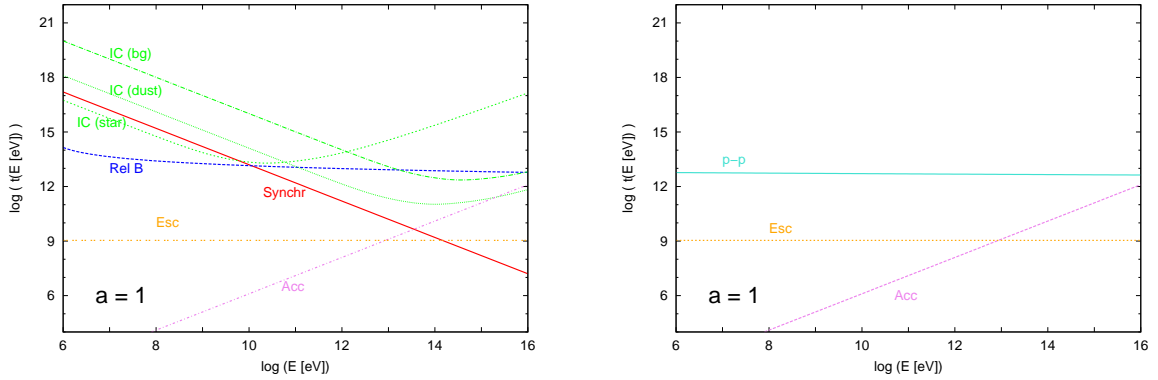


Figure 5: Left: acceleration (‘Acc’), escape (‘Esc’), and cooling times for electrons, due to synchrotron radiation (‘Synchr’), IC scattering of dust photons (‘IC (dust)’), stellar photons (‘IC (star)’), and background photons (‘IC (bg)’). Cooling time for relativistic Bremsstrahlung radiation is indicated as ‘Rel B’. The figure is for the case with equal energy density in electrons and protons ( $a = 1$ , see text). Right: acceleration, escape, and cooling time for protons due to the  $pp$  radiation process (‘p-p’).

## 4 Discussion and perspectives

The presence of highly relativistic particles in a dense medium with high photon density can result in the efficient generation of  $\gamma$ -rays. The corresponding  $\gamma$ -ray emissivity can be calculated using the delta-functional approximation (e.g. Aharonian & Atoyan 2000, Kelner et al. 2006).

In Fig. 6 we show the spectral energy distribution obtained for the case  $a = 1$ , with all contributions included (synchrotron self-Compton losses are negligible). The total luminosity from  $pp$  interactions is similar to that obtained from relativistic Bremsstrahlung of electrons. The IC up-scattering of IR photons is the major contribution at high energies, with a peak around 100 GeV. The detectability of the source by the Fermi LAT<sup>2</sup>  $\gamma$ -ray observatory will depend on the actual particle density and the contribution related to the secondary electrons at large  $a$ . The  $pp$  contribution extends well into the TeV regime, but its weaker and will be difficult to detect with the current ground-based Cherenkov telescope arrays.

For the case  $a = 100$ , the relativistic particle content is proton-dominated and  $\gamma$ -rays from  $pp$  process dominate the high energy spectrum. The CTA<sup>3</sup> North observatory might detect the source yielding information on the high energy cutoff.

<sup>2</sup>Fermi Large Area Telescope (<http://www-glast.stanford.edu/>).

<sup>3</sup>Cherenkov Telescope Array (<http://www.cta-observatory.org/>).

Observations of the spectral slope at high energies can be used to identify the proton content through the luminosity level, and the proton spectral index. Radio polarization data will provide additional information of  $B$ . X-ray observations will allow to determine the cutoff of the synchrotron spectrum, directly related to the maximum energy of the electrons<sup>4</sup>. This, in turn, would yield valuable information on the actual value of  $B$  and the correctness of the equipartition hypothesis.

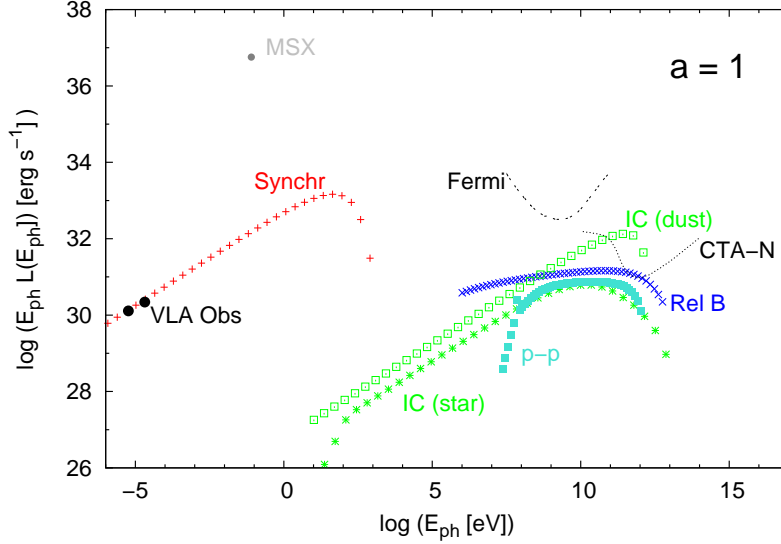


Figure 6: Spectral energy distribution for the case  $a = 1$ . Acronyms as in Figure 5. Measured radio fluxes from VLA observations ('VLA Obs') and MSX luminosity at D band are also represented. The contribution from secondary pairs is negligible in this case, so is not shown here.

## Acknowledgements

This work was supported by MinCyT - ANPCyT (PICT-2007-00848) and by CONICET (project ID 11220090100078). JM and GER acknowledge support by grant AYA2007-68034-C03-01 and -02 from the Spanish government and FEDER funds and Plan Andaluz de Investigación, Desarrollo e Innovación of Junta de Andalucía as research group FQM-322 and excellence fund FQM-5418.

## References

- Aharonian, F. A., Atoyan, A. M. 2000, *A&A*, 362, 937
- Comerón, F., Pasquali, A. 2007, *A&A*, 467, L23
- Condon, K. K., Cotton, W. D., Greisen, E. W., et al. 1998, *AJ*, 115, 1693
- Gies, D., Bolton, C. T. 1986, *ApJS*, 61, 419
- Hanson M. M. 2003, *ApJ* 97, 957-969
- Kelner, S. R., Aharonian, F. A., Bugayov, V. V. 2006, *Phys. Rev. D*, 74, 4081
- Kobulnicky, H. A., Gilbert, I. J., Kiminki, D. C. 2010, *ApJ*, 710, 529
- Van Buren, D., McCray, R. 1988, *ApJ*, 329, L93

<sup>4</sup>Notice that the situation is quite different from that of colliding winds, where the particle acceleration occurs in a region of high photon density, with dominance of IC losses.